High-temperature Oxidation Behaviour of MAX Phase Ceramics

Bai Cui, William Edward Lee

To understand the fundamental oxidation mechanisms in MAX phases the microstructural evolution of the oxide scales formed during oxidation over a range of temperatures was investigated. Two typical MAX phases, Ti_2AlC and Ti_2AlN, have been examined. In Ti_2AlC between 1100–1300 °C an outer rutile TiO_2 layer and a thicker, predominant and protective α-Al_2O_3 layer grow. Above 1400 °C the α-Al_2O_3 layer becomes cracked leading to loss of oxidation protection. In Ti_2AlN the oxidation is more complex involving formation of mixed rutile, anatase TiO_2 and Al_2O_3 layers which become dense from 900–1100 °C and under which a void layer forms possibly via the Kirkendall effect and gaseous NO_x release. With increasing temperature Al_2TiO_5 and a series of void layers additionally form.

High-temperature oxidation of MAX phases generally obeys a parabolic rate law, which can be explained by the diffusion-controlled mass transport mechanism during oxidation. The oxidation mechanism of Al-containing MAX phases involves selective oxidation of Al, leading to formation of continuous and protective Al_2O_3-rich scales on the substrates. Cracks may arise from stress generation in the oxide scale. Thermal stresses formed during cooling may result from thermal expansion mismatch of phases in the oxide scale, the high anisotropy of thermal expansion in Al_2TiO_5 and thermal expansion mismatch between the oxide scale and substrate. Growth stresses formed during isothermal oxidation treatment may arise from volume changes associated with oxidation reactions. Ti_2AlC and TiAlN could survive without oxidation damage and will potentially be tough below 1400 and 1200 °C, respectively. Improved knowledge of oxidation will lead to further use of these MAX phases in high temperature applications such as bearings, hot pressing dies, heating elements, corrosion resistant coatings and cladding materials for nuclear reactors.

1 Introduction

MAX phases are a family of ternary carbides and nitrides which show excellent mechanical properties and structural stability in extreme environments above 1000 °C, making them promising candidate materials for refractories, wear, aeronautic and nuclear applications. This paper introduces the range of MAX phases and their properties. However, high-temperature oxidation mechanisms in MAX phases are not fully understood which may limit their use in oxidising atmospheres. In this paper we also report studies of oxidation in typical MAX phases which may indicate possible methods of protecting them from oxidation at high temperature.

1.1 The MAX phases

MAX phases [1, 2] have general formula $M_{n+1}AX_n$, where M is an early transition metal (typically Ti, V, Cr, Nb and Ta), A is an A-group element (e.g. Si, Al, S, P, Sn, Ge and As), X is either C or N, and n runs from 1– 3. For n = 1 more than 50 M_2AX compounds (termed 211 phases) have been discovered; for n = 2 six M_3AX_2 compounds (312 phases) i.e. Ti_3SiC_2, Ti_3AlC_2, Ti_3GeC_2, Ta_3AlC_2, Ti_3SnC_2 and $(V_{0,5}Cr_{0,5})_3AlC_2$ have been identified; and for n = 3 five M_4AX_3 compounds (413 phases) i.e. Ti_4AlN_3, Ti_4GeC_3, Ta_4AlC_3, Nb_4AlC_3 and V_4AlC_3 have been found.

The family of MAX phases has been regularly added to since 2000. It is possible to form solid solutions from various ions on M-, A- and X-sites [1]. Among the solid solutions that form via the M-sites are: $(Ti,Cr)Al_2C$, $(Ti,V)_2SC$, $(Nb,Zr)_2AlC$, $(Ti,V)_2AlC$, $(Ti,Nb)_2AlC$, $(Ti,Ta)_2AlC$, $(V,Nb)_2AlC$, $(V,Ta)_2AlC$ and $(Ti,Hf)_2InC$. Solid solutions forming via the A-sites include $Ti_3(Ge,Si)C_2$ and $Ti_3(Si,Al)C_2$. Solid solutions that form via the X-sites in-

Bai Cui, William Edward Lee
Centre for Advanced Structural Ceramics
Department of Materials
Imperial College London
London SW7 2AZ
Great Britain

Corresponding author: *Bai Cui*
E-mail: cuibai@illinois.edu

Keywords: MAX phase, ceramics, oxidation, microstructure

Received: 05.06.2012
Accepted: 17.09.2012

(This paper is partly based on Bai Cui's PhD Dissertation, Imperial College London, 2011)

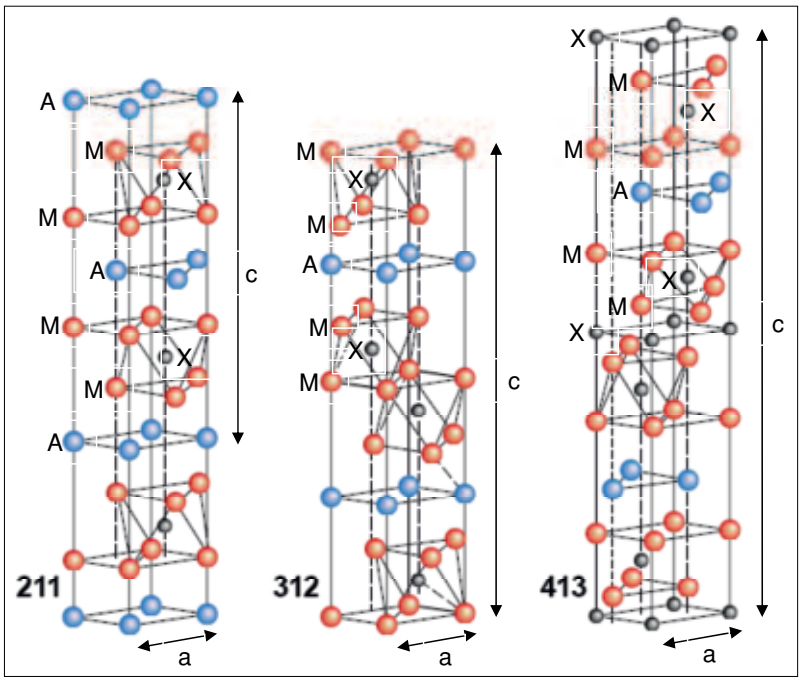

Fig. 1 Crystal structures of 211, 312 and 413 MAX phases. Unit cells are indicated by lattice parameters labeled a and c. Revised from [1]

clude a continuous series of solid solutions $Ti_2AlC_{0,8-x}N_x$ (x = 0 – 0,8) occurs at 1490 °C [3].

All MAX phases are reported to crystallize in layered hexagonal crystal structures with space group $P6_3/mmc$ (Fig. 1). The layered structure consists of repeated $M_{n+1}X_n$ slabs and planar-packed A-group atoms. The $M_{n+1}X_n$ slabs have a NaCl-type cubic structure similar to that of the corresponding MX binary carbides while X atoms coordinated in octahedral position of M atoms. A-group atom planes intercalate between twinned MX layers.

Many mechanical and structural features of $M_{n+1}AX_n$ ceramics are inherited from their binary counterparts, e.g. TiC, TiN, SiC and Si_3N_4, while many more novel properties emerge because of new chemical bonds and atomic coordination at the boundaries of different slabs. MAX phases have shown unusual mechanical properties combining those of both ceramics and metals, such as damage tolerance, high elastic stiffness and microscale ductility [4]. These properties are rarely exhibited by their binary counterparts. The physical origin of the unusual mechanical properties is their layered characteristics at the atomic scale. The first ab initio calculation on MAX phases was reported by *Medvedeva et al.* [5]. The damage tolerance of Ti_3SiC_2 was explained for the first time by a weak coupling between the Ti_3C_2 layers and the Si atomic planes. Since that time, the chemical bonding characteristics of MAX phases and their relation with properties have been comprehensively investigated. Important conclusions can be summarized as follows [1, 2]:

- The M and X atoms form strong directional covalently bonded $(M\text{-}X)_n$-M chains in the M-X layers which contribute to the refractoriness and high elastic stiffness. The M-X bonds are comparable to those in the MX binary counterparts.
- M-A bonds are somewhat weaker than M-X bonds and are able to stretch and compress under shear deformation. There is strong overlap between the A *p* orbitals and M *d* orbitals.
- The M *d*-M *d* metallic bonding states dominate the density of states at the Fermi level and thus MAX phases show metallic-type electrical conductivity. The high conductivity originates predominantly from the *d-d* bonding between transition-metal atoms coordinated to A-group atoms.

At elevated temperatures, MAX phases usually undergo decomposition prior to melting. Generally, $M_{n+1}AX_n$ ceramics decompose according to [1]:

$$M_{n+1}AX_n\,(s) \rightarrow M_{n+1}AX_n(s) + A\ (s\ or\ l) \quad (1)$$

where *s* denotes solid phase and *l* denotes liquid. This decomposition mode is usually explained by the high activity of A in the structure, derived from the fact that the bonding between M and A is weaker than that between M and X. Therefore, elemental "A" escapes from the substrate and only $M_{n+1}X_n$ remains. Decomposition temperatures (T_d) of MAX phases vary widely as summarized in Tab. 1. Even at room temperature, Cr_2GaN was observed to extrude gallium filaments several centimetres long [6]. The phase stability of MAX phases is believed to be closely related to the behaviour

Tab. 1 Summary of decomposition temperatures (T_d) of typical MAX phases. The melting points (T_m) of other main phases in the Ti-Al-C and Ti-Al-N ternary systems are also listed. All the T_d data of MAX phases are measured in Ar atmosphere or under vacuum (V)

(a) MAX phases

	Ti_2AlC	Ti_3AlC_2	Ti_2AlN	Ti_4AlN_3	Cr_2GaN	Cr_2AlC	Ti_3SiC_2
T_d [°C]	1625 ±10 (Ar)[8]	1360 (Ar)[8] <1400 (V)[9]	>1500 (V)[10]	>1400 (V)[11]	850 (V)[1]	1524 (Ar)[12]	>1800 [13] 2200 ±20 [1](Ar)

(b) Other main phases in Ti-Al-C system [8]

	Ti	Al	C[1]	TiAl	Ti_3Al	$TiAl_3$	$TiAl_2$	TiC_{1-x}	Al_4C_3	Ti_3AlC
T_m [°C]	1670	660	2776	1462	1164	1393	1200	3066	2173	1580 ±10

1 Graphite.

(c) Other main phases in Ti-Al-N system [7, 11]

	Ti	Al	TiAl	Ti_3Al	$TiAl_3$	$TiAl_2$	TiN_{1-x}	AlN	Ti_3AlN
T_m [°C])	1670	660	1462	1164	1393	1200	3061	2432	>1300

of A-group atoms, as well as to the inherently weak M-A bonds. By contrast, the transition-metal carbide slabs are stable because of the strong covalent bonds between M and C atoms.

Phase diagrams graphically illustrate the stability of MAX phases. Fig. 2 shows Ti-Al-N isothermal sections (N corner is not shown) at 1000 °C and 1325 °C from the Al-N-Ti ternary phase diagram [7]. MAX phases, i.e. Ti_2AlN (τ_2) and $Ti_4AlN_{2,9}$ (τ_3), are only stable in a very narrow region. Note Ti_3AlN_{1-x} (τ_1), which has a perovskite-type cubic structure, does not belong to the family of MAX phases. All these ternary phases occupy a small area in the isothermal sections, which means that they are stable over a narrow compositional region at high temperatures.

1.2 Oxidation of a MAX phase

As many refractories, nuclear and aerospace applications involve direct or indirect exposure to oxidizing atmospheres, all nonoxide materials will undergo oxidation to form some combination of solid, liquid, or gaseous reaction product [14]. It is the oxidation behaviour that is thus a primary property associated with the materials selection process of these high-temperature ceramics. Oxidation of ceramics is a class of engineering corrosion involving gases. The temperature range for oxidation can be classified as ultra-high temperature (>2000 °C), high-temperature (1000–2000 °C), intermediate temperature (500–1000 °C) and low temperature (0–500 °C). Oxidation of ceramics has been studied under both isothermal (i.e. at constant temperature) and cyclic (i.e. cyclic heating and cooling) conditions.

Oxidation reactions may be passive, in which case a protective oxide layer forms, or active, where the reaction continues until the body is completely oxidized. The design of oxidation-resistant materials depends on the presence of an element which can oxidize and form a thin, adherent and protective oxide layer on exposure to oxygen. Few elements form oxides that are protective enough to be useful oxidation barriers at temperatures above 1000 °C. Most notable oxides are those of Si, Al and Cr. Formation of Al_2O_3 in general gives better high temperature protection than SiO_2 or Cr_2O_3 [15]. Many MAX phases contain Si, Al or Cr, such as Ti_2AlC, Ti_2AlN, Cr_2AlC, Ti_3AlC_2 and Ti_3SiC_2. The high-temperature oxidation behaviour of the first two compounds is the focus of this paper.

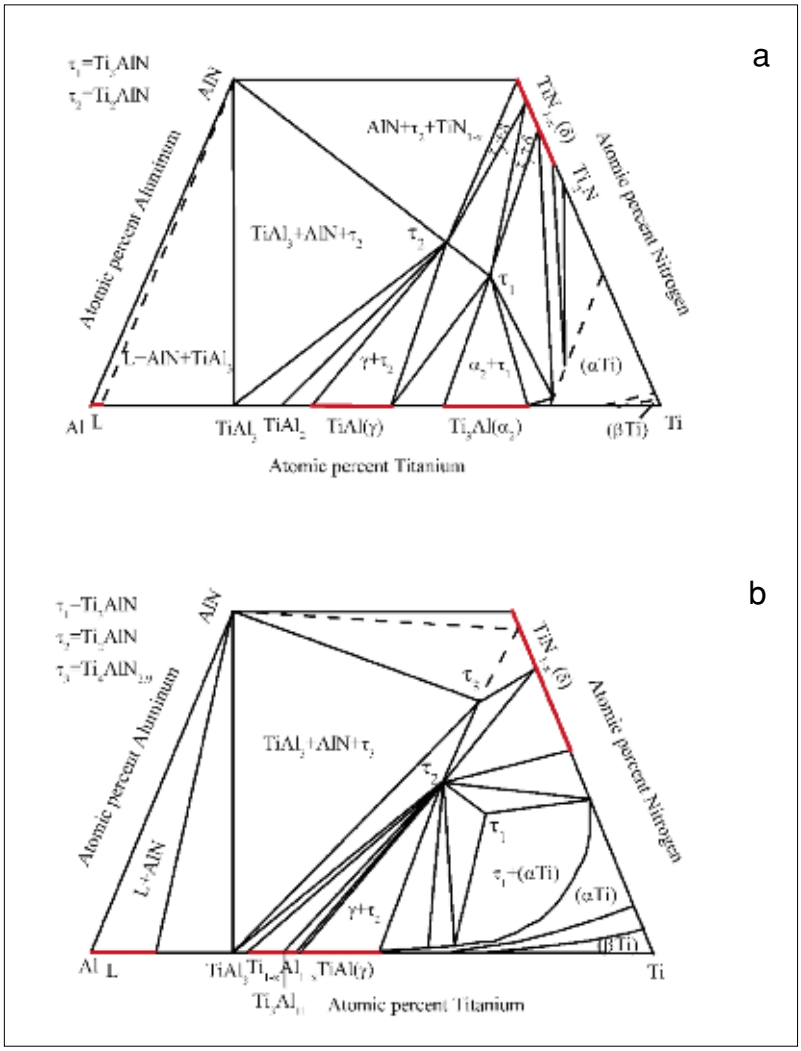

Fig. 2 Ti-Al-N ternary phase diagram: isothermal section (N corner not shown) at (a) 1000 and (b) 1325 °C, respectively. MAX phases, i.e. Ti_2AlN (τ2) and $Ti_4AlN_{2,9}$ (τ3), are stable in a very narrow compositional region at high temperature. Redrawn from [7]

1.2.1 Oxidation kinetics

Kinetic theory is concerned primarily with the progress of a reaction with time. Thus, the first task is to find relationships between oxidation and time. Empirically, the growth of the oxide layer as a function of time generally can be represented by one of the following equations [16] for thick films:

$y = kt$ (linear relationship) (2)

$y^2 = kt$ (parabolic relationship) (3)

$y^3 = kt$ (cubic relationship) (4)

where y is the film thickness, t is time, k is the rate constant. Oxidation processes are often more complex than the simple mechanism of a single species diffusing through an oxide layer. Combinations of two or more of the relationships listed above in a single oxidation-time curve are also quite common. Some ceramics, metals and alloys are observed to start to oxidize parabolically and then continue linearly [16].

Oxidation kinetics of ceramics are usually studied using thermogravimetry (TG) to measure mass change as a function of time at the oxidation temperature. This is why in the literature, oxidation kinetics are often given as the mass change per unit area for a unit time. This can be converted to the thickness of the oxide per unit time by dividing by the density of the oxides.

High-temperature oxidation of MAX phases generally obeys a parabolic rate law. TGA analysis is usually conducted to evaluate the oxidation kinetics from continuous-isothermal-mass-change measurements. The rela-

Tab. 2 Summary of parabolic rate constants (k_p) and the apparent activation energy (Q) for the high temperature oxidation of typical MAX phases and a typical oxidation-resistant alloy, Ni-52Al at 1000–1400 °C in air [2]

Temperature [°C]	Parabolic Rate Constants, k_p [$kg^2m^{-4}s^{-1}$]					
	Ti_2AlC	Cr_2AlC	Ti_3AlC_2	$Ti_3Si_{0,9}Al_{0,1}C_2$	Ti_3SiC_2	Ni-52Al
1000	$7,8 \times 10^{-11}$	$1,1 \times 10^{-11}$	$4,1 \times 10^{-11}$	$3,2 \times 10^{-11}$	$2,4 \times 10^{-9}$	$2,1 \times 10^{-11}$
1100	$2,8 \times 10^{-10}$	$2,3 \times 10^{-10}$	$2,7 \times 10^{-10}$	$1,2 \times 10^{-10}$	$4,0 \times 10^{-7}$	$8,9 \times 10^{-11}$
1200	$1,1 \times 10^{-9}$	$5,6 \times 10^{-10}$	$4,2 \times 10^{-10}$	$4,0 \times 10^{-10}$	$2,2 \times 10^{-6}$	$6,7 \times 10^{-10}$
1300	$1,8 \times 10^{-9}$	$3,0 \times 10^{-9}$	$1,1 \times 10^{-9}$	$2,4 \times 10^{-9}$	$9,6 \times 10^{-6}$	$1,6 \times 10^{-9}$
1400	–	–	$1,7 \times 10^{-8}$	–	–	–
Q [kJ mol^{-1}]	182	298	175	234	450	251

tionship between (W/A)^2 and oxidation time is approximately linear, which can be described as:

$$(W/A)^2 = k_P t \quad (5)$$

where W is mass increase, A is surface area, k_p is parabolic oxidation rate constant, t is oxidation time. The parabolic rate law can be explained by the mass transport mechanism during oxidation which is generally accepted to be diffusion controlled [16]. A parabolic law assumes that the rate of oxi-dation is controlled by diffusion through the oxide scale.

The parabolic rate constants for the high-temperature oxidation of typical MAX phases are summarized in Tab. 2. Judging from the data, Ti_2AlC, Cr_2AlC and Ti_3AlC_2 have good oxidation resistance, which is comparable to that of an oxidation-resistant alloy, Ni-52Al [17]. The parabolic rate constants of Ti_3AlC_2 are two to four orders of magnitude lower than those of Ti_3SiC_2 at the same temperature, suggesting Ti_3AlC_2 has much better oxidation resistance than Ti_3SiC_2. However, by substituting a small amount of Si with Al, the parabolic rate constants of $Ti_3Si_{0,9}Al_{0,1}C_2$ solid solution become the same order of magnitude as those of Ti_3AlC_2 [18].

The parabolic rate constant and temperature can be generally correlated according to an *Arrhenius*-type equation [1]:

$$k_P = k_0 \exp(-Q / RT) \quad (6)$$

where k_0 is the pre-exponential factor, R the universal gas constant, T the absolute temperature, and Q the apparent activation energy. However, Q could be referred to as activation energy only in cases where the rate-controlling step is well defined. As the nature of the diffusion medium may vary with temperature, the oxidation rate can also vary and Q values can change. Q is thus only a temperature coefficient and not true activation energy [2]. Equation 6 can be rewritten as:

$$\ln k_P = \ln k_0 \exp(-Q / R)(1 / T) \quad (7)$$

According to Equation 7, Q can be determined from the slope of the $lnk_p vs 1/T$ plot. The last row of Tab. 2 lists Q values of MAX phases.

1.2.2 Common features of oxidation mechanisms

The oxidation mechanism of Al-containing MAX phases generally involves selective oxidation of Al, leading to formation of continuous and protective Al_2O_3-rich scales on the substrates [1, 2]. Al, an "A" element, is found to be weakly bonded in these MAX phases. The M-X bonding in MAX phases is strongly covalent, whereas the M-A bonding is relatively weak. Strong reaction between M and X would decrease the activity of M and result in an increased activity of A. No observable Al-depleted, Ti-enriched or O-enriched zones have been observed in the Ti_2AlC or Ti_3AlC_2 substrates during high-temperature oxidation [2], suggesting that Al in the substrate has a high diffusivity and oxygen solubility in the substrate is negligible.

Vacancy-mediated diffusion is of great importance in the oxidation mechanism of high-temperature materials and the mechanism involved is believed to be indispensable for comprehending the kinetic behaviour of these materials [16]. Theoretical investigation has demonstrated that the energy barriers involved in the vacancy migration in Ti_2AlC are 0,83, 2,38 and 3,00 eV, for V_{Al}, V_{Ti} and V_C-assisted diffusion, respectively [24]. These results suggest that vacancy-mediated diffusion in Ti_2AlC is most energetically favourable for V_{Al}. Under an oxidizing environment, Al atoms would diffuse outward via vacancy-mediated diffusion to form a protective Al_2O_3 scale. Theoretical investigation of the phase stability of Ti_2AlC containing Al vacancies [25] predicts that Ti_2AlC can preserve its crystal structure down to a sub-stoichiometry of $Ti_2Al_{0,5}C$. This Ti_2Al_xC phase has been experimentally observed recently [21]. As a result of preferential migration of Al atoms from the Ti_2AlC substrates, Al vacancies exist while Ti_2AlC preserves its crystal structure after long-term exposure in air, providing sufficient Al atoms for formation of a protective Al_2O_3 scale.

2 Results and discussions

2.1 Microstructural evolution

Let the clean surface of a ceramic be exposed to the attack of a gas such as oxygen [16]. The reaction will begin at the ceramic-gas surface, and unless the reaction products are volatile, an intermediate oxide layer will form between the ceramic and the gas. This oxide layer may be compact or interspersed with pores or cracks, so that further reaction may involve atomic diffusion or simply passage of gas molecules through the pores. Diffusion may be through the grains, along grain boundaries or surfaces. When a ceramic reacts, either one or all of its elements may form oxides by reaction with the gas, and the resulting layer may be a mixture of different particles or clearly subdivided into individual layers. The latter may apply to a ceramic that forms several stable oxides of different composition with the oxygen.

To understand the mechanism of oxidation of ceramics, the phase composition and microstructures of the oxide scale must be studied. The phases formed in the oxide scale are often identified by using X-ray or neutron diffraction. The microstructures are revealed by optical or electron microscopy of plan view and cross-section samples to show the air-scale and scale-ceramic interfaces. The microstructures are usually characterized post mortem at room temperature from the cooled or quenched sample. Dynamic, in situ studies are being attempted but particularly at high-temperature are empirically difficult [19].

The observations of the microstructural evolution may be different, likely due to different as-made ceramic microstructures, impurity contents, temperatures, times and atmospheres. The microstructural evolution of Ti_2AlC and Ti_2AlN MAX phases from the authors' research are presented and discussed here.

2.1.1 Ti_2AlC oxidation

Based on XRD analysis, the oxidation of Ti_2AlC may occur via the reactions:

$$Ti_2AlC + \frac{15}{4}O_2 \rightarrow 2TiO_2\,(rutile) + \frac{1}{2}\alpha - Al_2O_3 + CO_2$$
$$V = 59{,}0\ \%,\ m = 56{,}4\ \%\ (T > 900\ ^\circ C) \qquad (8)$$

where V is volume change and m mass change on reaction. Gaseous products are CO_2 or CO. At the air/oxide scale interface, CO_2 is likely formed due to the high oxygen pressure. At the Ti_2AlC/oxide scale interface, CO is likely formed due to the low oxygen pressure.

At 1400 °C, TiO_2 (rutile) and α-Al_2O_3 react to form Al_2TiO_5:

$$TiO_2 + Al_2O_3 \rightarrow Al_2TiO_5$$
$$V = 10{,}8\ \%,\ m = 0\ \% \qquad (9)$$

SEM and TEM investigations reveal the microstructural evolution of the oxide scale on Ti_2AlC, as suggested in Fig. 3 [20]. At 900 °C (Fig. 3a), the oxide scale consisted of a TiO_2-rich outer layer and an Al_2O_3-rich inner layer, formed by faster outgrowth of TiO_2 than Al_2O_3. An intermediate layer formed between the oxide scale and substrate is an Al depleted layer consisting of nonstoichiometric Ti_2Al_xC ($x < 1$) nanocrystallites (< 20 nm) transforming from Ti_2AlC due to depletion of Al [21]. At 1000 °C (Fig. 3b), over most of the Ti_2AlC surface, a thin (about 1 µm) alumina oxide layer was formed. In addition, thick asperities (1–4 µm thick) consisting an outer TiO_2 layer and an inner alumina layer are distributed over the oxide scale at intervals of several microns. The oxidation of Ti_2AlC in thick asperities is enhanced relative to that in the thin layers. This behaviour may be explained by the presence of defects and cracks (induced by polishing) at the positions of the asperities on the original Ti_2AlC surface, which decreased the activation energy for oxidation. At 1100–1300 °C (Fig. 3c), a uniform and continuous oxide scale was formed consisting an outer TiO_2 layer and an inner alumina layer. At 1400 °C (Fig. 3d), the oxide scale became cracked.

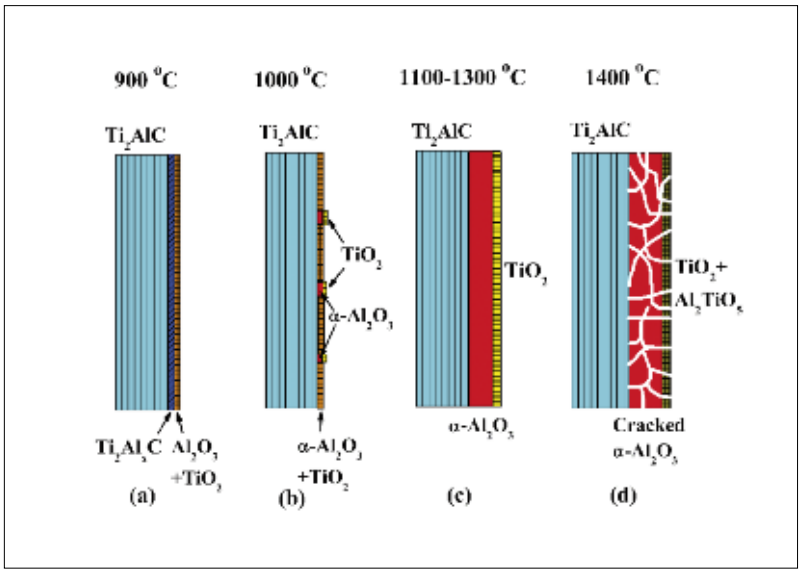

Fig. 3 Schematic illustration summarizing the microstructural evolution during Ti_2AlC oxidation. Revised from [20]

2.1.2 Ti_2AlN oxidation

XRD analysis suggests that oxidation of Ti_2AlN occurs via the reactions [22]:

$$Ti_2AlN + O_2 \rightarrow TiO_2\,(rutile) + TiO_2\,(anatase) + \alpha - Al_2O_3 + NO_x$$
$$V = 59{,}5\ \%,\ m = 54{,}1\ \%\ (T < 1200\ ^\circ C) \qquad (10)$$

$$Ti_2AlN + O_2 \rightarrow TiO_2\,(rutile) + \alpha - Al_2O_3 + Al_2TiO_5 + NO_x$$
$$V = 59{,}5 \sim 76{,}7\ \%,\ m = 54{,}1\ \%\ (T < 1200\ ^\circ C) \qquad (11)$$

Where NO_x ($x = 1–2$) refers to the gaseous oxidation products of Ti_2AlN. In Equation 11, V increased with increased Al_2TiO_5 formation. α-Al_2O_3 and two polymorphs of TiO_2, anatase and rutile, form in the oxide scale at or above 900 °C. At 1200 °C, all anatase has been transformed to rutile. Al_2TiO_5 arises at 1200 °C formed by reaction between TiO_2 and Al_2O_3.

Microstructural development during Ti_2AlN oxidation characterised by SEM and TEM investigations [22], is shown schematically in Fig. 4. At 900 °C, the oxide scale microstructure consisted of an outer dense layer (1–2 µm thick) and an inner porous layer (1–2 µm thick). In the dense layer angular TiO_2 grains (<100 nm) were distributed in a dense α-Al_2O_3 grain (<100 nm) matrix. In the porous layer loose angular TiO_2 grains (~100 nm) were predominant. At 1000 °C, the outermost layer was dense TiO_2, over dense α-Al_2O_3. The innermost porous layer was a mixture of TiO_2 and α-Al_2O_3 and the Ti/Al atomic ratio is close to 2:1. A number of submicron pores are distributed uniformly in this porous layer. At 1200 °C, the outmost dense layer was a mixture of TiO_2, α-Al_2O_3 and Al_2TiO_5 and the Ti/Al atomic ratio is close to 2:1. A continuous void layer formed below the dense layer. The void layer is likely developed due to the *Kirkendall* effect by rapid inward diffusion of Al [23] and gaseous NO_x release. The inner porous layer was a mixture of TiO_2, α-Al_2O_3 and Al_2TiO_5 and the Ti/Al atomic ratio is close to 1:1. At 1300 °C, the outmost dense layer was a mixture of TiO_2, α-Al_2O_3 and Al_2TiO_5 and the Ti/Al atomic ratio is close to 2:1. A continuous void layer formed below the dense layer. Below the void layer was a porous layer which was a mixture of TiO_2, α-Al_2O_3 and Al_2TiO_5 and the Ti/Al atomic ratio is close to 1:1. A second continuous void layer formed below the porous layer. Below the second void layer was a porous layer which was a mixture of TiO_2, α-Al_2O_3 and Al_2TiO_5 and in hich the Ti/Al atomic ratio is close to 1:1. The inner layer adjacent the Ti_2AlN substrate was a porous TiO_2 layer. At 1400 °C, the outmost

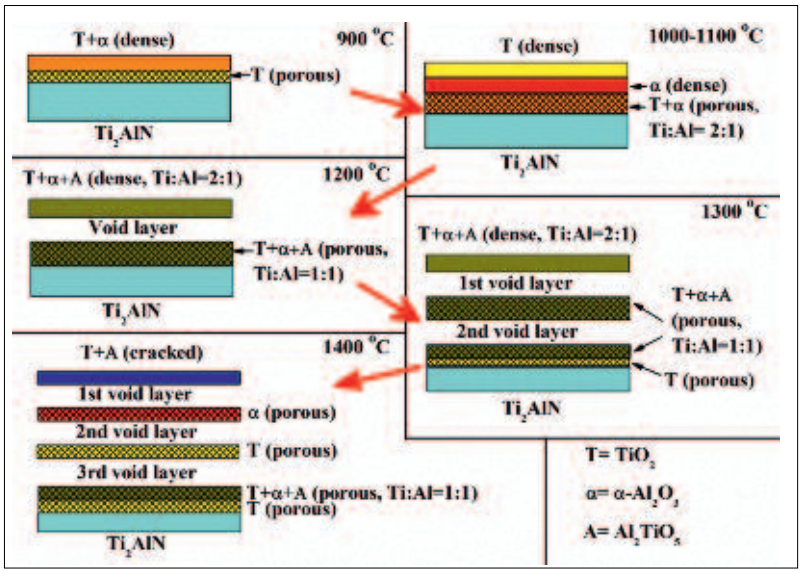

Fig. 4 Schematic illustration of oxide scale formation during Ti_2AlN oxidation. Revised from [22]

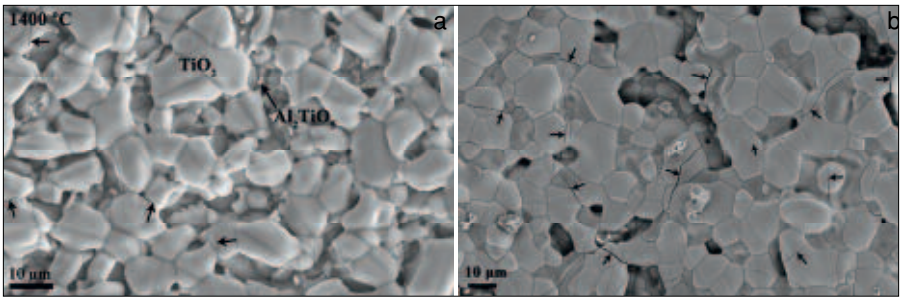

Fig. 5 Cracks formed in the surface TiO_2 grains after Ti_2AlC oxidation at 1400 °C for 1 h (a) and 10 h (b), respectively, and then air cooling to room temperature. The crack density is (a) 0,0082 ± 0,0010 µm^{-2}; (b) 0,0106 ± 0,0008 µm^{-2}. Short arrows indicate cracks

dense layer was a mixture of TiO_2 and Al_2TiO_5. A continuous void layer formed below the dense layer. Below the void layer was a porous α-Al_2O_3 layer. A second void layer formed below the α-Al_2O_3 layer. Below the second void layer was a porous TiO_2 layer. A third void layer formed below the TiO_2 layer. Below the third void layer was a mixture of TiO_2, α-Al_2O_3 and Al_2TiO_5. A porous TiO_2 layer formed adjacent the substrate. During Ti_2AlN oxidation, complex microstructures of the oxide scale may be formed. Porous and void layers formed due to the Kirkendall effect and gaseous NO_x release. Multilayer microstructure formed firstly by demixing resulting from different growth kinetics of each oxide, and secondly by voids providing channels for the rapid ingress of oxygen. A new cycle of oxidation started from the void layer, resulting in repeated layers of oxide scale.

Tab. 3 Summary of thermal properties of typical MAX phases and their oxidation products (Al_2O_3, TiO_2 and Al_2TiO_5)

	Ti_2AlC	Ti_3AlC_2	Ti_2AlN	α-Al_2O_3	TiO_2 (Rutile)	Al_2TiO_5
T_d [°C] T_m [°C]	1625 ± 10	1360	>1500	2072	1840	1860
Thermal conductivity [W·m^{-1}·K^{-1}] at 300 K	33 46 [2]	40 [2]	–	30–35	11,7	1,5 [27]
TEC [10^{-6}·K^{-1}] (25–1200 °C)	α_a = 7,1 ± 0,3 α_c = 10 ± 0,5 8,2 ± 0,2[1] 8,8 ± 0,2[1] [1,2]	α_a = 8,3 ± 0,1 α_c = 11,1 ± 0,1 9,0 ± 0,2[1] 9,2 ± 0,1[1] [1,2]	α_a = 8,6 ± 0,2 α_c = 7,0 ± 0,5 8,2 ± 0,2[1] [1]	α_a = 7,9 α_c = 8,8	α_a = 9,2 α_c = 7,1	α_a = 10,9 α_b = 20,5 α_c = -2,7 [27]

α_a is normal to the c-axis, and α_c is parallel to the c-axis
[1] average TEC value

2.2 Stress generation during oxidation

Stress generation in the oxide scale developed on high temperature materials may induce scale cracking and spalling, which in turn, leads to loss of protective properties and accelerates material degradation. Stresses can be generated during cooling (i.e. thermal stresses) and during the isothermal oxidation treatment (i.e. growth stresses) [26]. The following discussion takes Ti_2AlC as an example. After Ti_2AlC oxidation at 1400 °C and then air cooling to room temperature, cracks developed in the surface TiO_2 grains (Fig. 5). The formation of cracks may be related to stress generation in the oxide scale. Before the stress generation is discussed, it is necessary to clarify the phases and their thermal expansion coefficients (TEC) in the oxide scale after Ti_2AlC oxidation (Tab. 3). Now thermal and growth stresses in turn are discussed. Firstly, the thermal stresses formed in the oxide scale during cooling may have three origins, as discussed below:

a) From TEC mismatch of the phases in the oxide scale (TiO_2, Al_2O_3 and Al_2TiO_5).
Because the oxide scale is a mixture containing TiO_2, Al_2O_3 and Al_2TiO_5, a simplified model for the multiphase materials developed by *Eshelby* might apply. For simplicity, consider a two-phase system where one phase can be regarded as an inclusion and the other as the matrix, with the TEC α_i and α_m, respectively. At equilibrium, the thermal stress can be given by [28]:

$$\sigma_{i,eq} = \sigma_{m,eq} = \frac{\Delta\alpha\Delta T}{1/E_i + 1/E_m} = \frac{(\alpha_m - \alpha_i)\Delta T}{1/E_i + 1/E_m} \quad (12)$$

Where E_i and E_m are Young's modulus of the inclusion and the matrix, respectively. T is temperature difference.

In the oxide scale after Ti_2AlC oxidation, the small difference of TEC of rutile and α-Al_2O_3 suggests that below 1300 °C, the thermal stress is small. At 1400 °C, the TEC mismatch of rutile and α-Al_2O_3 is small while those of TiO_2-Al_2TiO_5 and α-Al_2O_3-Al_2TiO_5 are significant, and so the thermal stresses generated by these TEC mismatches are significant.

b) From high anisotropy of TEC in Al_2TiO_5.
Thermal stress can be also induced by anisotropy in the TEC of single-phase solids [28]. The high anisotropy of TEC in Al_2TiO_5 ($\alpha_a = 10{,}9 \times 10^{-6}$ K^{-1}, $\alpha_b = 20{,}5 \times 10^{-6}$ K^{-1}, $\alpha_c = -2{,}7 \times 10^{-6}$ K^{-1}, 0–1273 K) is known to trigger spontaneous microcracking upon cooling when a critical grain size is exceeded. A grain size effect has been observed in the microcracking of Al_2TiO_5. The microcracking becomes less severe with decreasing grain size, and below a critical grain size, it is no longer observed. The critical grain size, d_{crit}, is [28]:

$$d_{crit} = k\frac{G_{c,gb}}{E(\Delta\alpha\Delta T)^2} \qquad (13)$$

Where k is a constant, $G_{c,gb}$ is the grain boundary fracture toughness, E is *Young*'s modulus, α is the maximum anisotropy of the thermal expansion coefficient, and T is the temperature difference. In this research, $T = 1400 - 25 = 1375$ °C. Given that for Al_2TiO_5, $G_{c,gb} = 0{,}5$ J m^{-2}, $Y = 250$ GPa, $k = 184$ µm °C^{-2}, and $\alpha = 23{,}2$ K^{-1}. The critical grain size, d_{crit}, is calculated from Equation 13 to be 0,4 µm. After Ti_2AlC oxidation at 1400 °C, the Al_2TiO_5 grain size observed is about 1,2 µm, much larger than the critical grain size. Therefore, it is possible that the crack formation is triggered by microcracking caused by high anisotropy of TEC in Al_2TiO_5 upon cooling from 1400 °C.

c) From the TEC mismatch between the oxide scale and Ti_2AlC substrate.
Since the oxide scale thickness is much smaller than that of Ti_2AlC substrate, it is considered that the oxide scale is under in-plane stress conditions [29]. The theoretical in-plane stress can be estimated from:

$$\sigma_{ox} = -\frac{E_{ox}}{(1-\nu_{ox})}\frac{(\alpha_{ox}-\alpha_s)\Delta T}{1+\frac{E_{ox}(1-\nu_s)}{E_s(1-\nu_{ox})}\frac{h_{ox}}{h_s}} \qquad (14)$$

where subscripts *ox* and *s* refer to oxide scale and substrate, respectively and *h* represents the thickness. Rutile and α-Al_2O_3 have small TEC differences from Ti_2AlC while Al_2TiO_5 has a large difference (Tab. 3). Consequently, the oxide scale average TEC (a mixture of rutile and α-Al_2O_3) below 1300 °C is close to that of the Ti_2AlC substrate, while that of the oxide scale (a mixture of rutile, α-Al_2O_3 and Al_2TiO_5) at 1400 °C is significantly different. As a result, the thermal stress between the oxide scale and Ti_2AlC substrate is small below 1300 °C, and significant at 1400 °C.
Secondly, the growth stresses formed in the oxide scale during the isothermal oxidation treatment may arise from the volume changes associated with oxidation reactions of Ti_2AlC (Equations 8 and 9). The stresses arising from volume changes can be approximated by [28]:

$$\sigma \approx \frac{E}{3(1-2\nu)}\frac{\Delta V}{V_0} \qquad (15)$$

where V and V_0 are volume change and original volume, respectively. The growth stresses increase proportionally with V. Therefore, after Ti_2AlC oxidation the growth stresses increased with temperature because formation of significant amounts of oxide products generated large volume changes according to Equations 8. The growth stresses are larger at 1400 °C because formation of more significant amounts of Al_2TiO_5 generated additional volume changes according to Equation 9.
Combining thermal and growth stresses reveals on Ti_2AlC oxidation the stresses generated at 1400 °C are significantly larger than those below 1300 °C. After heating to 1400 °C and then air cooling to room temperature, cracks (Fig. 5) developed in surface TiO_2 grains. Therefore, crack formation is directly related to the significantly large stresses at 1400 °C.
It has shown that Ti_2AlC could survive without oxidation damage and will potentially be tough below 1400 °C, while Ti_2AlN could survive below 1200 °C [22]. They are thus be expected to operate successfully in many target applications in refractories, such as high-temperature bearings, hot pressing dies, glove formers, electric heating elements (Maxthal® developed by *Kanthal AB*) [30], high-temperature electrodes, corrosion resistant coatings, exhaust gas catalyst supports for automobiles, and cladding materials for lead cooled fast breeder nuclear reactors [31].

3 Conclusions

(1) During Ti_2AlC oxidation between 1100–1300 °C an outer rutile TiO_2 layer and a thicker, predominant and protective α-Al_2O_3 layer grow. Above 1400 °C Al_2TiO_5 forms on reactions between TiO_2 and the α-Al_2O_3 layer becomes cracked leading to loss of oxidation protection.
(2) In Ti_2AlN the oxidation is more complex involving formation of mixed rutile, anatase TiO_2 and Al_2O_3 layers which become dense from 900–1100 °C and under which a void layer forms possibly via the Kirkendall effect by the rapid outward diffusion of Al and gaseous NO_x release. With increasing temperature Al_2TiO_5 and a series of void layers additionally form. The multilayer microstructure developed firstly by demixing due to different growth kinetics of each oxide, and secondly by voids providing channels for the rapid ingress of oxygen.
(3) The kinetics for high-temperature oxidation of MAX phases generally obeys a parabolic rate law, which can be explained by the diffusion controlled mass transport mechanism during oxidation. The oxidation mechanism of Al-containing MAX phases involves selective oxidation of Al. Al has a relatively high diffusivity due to the defect structure of MAX phases. This can cause formation of continuous and protective Al_2O_3-rich scales on the substrates.
(4) Cracks propagate in TiO_2 grains after Ti_2AlC oxidation at 1400 °C, providing channels for rapid ingress of oxygen to the body, leading to extensive heavy oxidation above 1400 °C. Formation of cracks may arise from stress generation in the oxide scale. The thermal stresses formed during cooling may result from thermal expansion mismatch of phases (TiO_2, Al_2O_3 and Al_2TiO_5) in the oxide scale, the high anisotropy of thermal expansion in Al_2TiO_5 and thermal expansion mismatch between the oxide scale and Ti_2AlC substrate. Growth stresses formed during isothermal oxidation treatment may arise from the volume changes associated with oxidation reactions of Ti_2AlC.

References

[1] Barsoum, M.W.: The $M_{n+1}AX_n$ phases: a new class of solids; thermodynamically stable nanolaminates. Progress in Solid State Chemistry **28** (2000) [1–4] 201–281

[2] Wang J.; Zhou Y.: Recent progress in theoretical prediction, preparation, and characterization of layered ternary transition-metal carbides. Annual Rev. of Mater. Res. **39** (2009) [3] 415–443

[3] Barsoum, M.W.; El-Raghy, T.; Ali, M.: Processing and characterization of Ti_2AlC, Ti_2AlN, and $Ti_2AlC_{0.5}N_{0.5}$. Metallurgical and Mater. Transactions A **31** (2000) [7] 1857–1865

[4] Eklund, P. et al.: The $M_{n+1}AX_n$ phases: materials science and thin-film processing. Thin Solid Films **518** (2010) [8] 1851–1878

[5] Medvedeva, N.I. et al.: Electronic properties of Ti_3SiC_2-based solid solutions. Phys. Rev. B **58** (1998) [24] 16042–16050

[6] Barsoum, M.W.; Farber, L.: Room-temperature deintercalation and self-extrusion of Ga from Cr_2GaN. Science 284, no. 5416 (1999) 937–939

[7] Raghavan, V.: Al-N-Ti (Aluminum-Nitrogen-Titanium). J. of Phase Equilibria and Diffusion **27** (2006) [2] 159–162

[8] Pietzka, M.A.; Schuster, J.C.: Summary of constitutional data on the aluminum-carbon-titanium system. J. of Phase Equilibria and Diffusion **15** (1994) [4] 392–400

[9] Pang, W.K.; Low, I.M.; Sun. Z.M.: In situ high-temperature diffraction study of the thermal dissociation of Ti_3AlC_2 in vacuum. J. Amer. Ceram. Soc. **93** (2010) [9] 2871–2876

[10] Pang, W. et al.: In situ diffraction study on decomposition of Ti_2AlN at 1500–1800 °C in vacuum. Mater. Sci. Engin. A **528** (2010) [1] 137–142

[11] Schuster, J.; Bauer, J.: The ternary system titanium-aluminum-nitrogen. J. of Solid State Chem. **53** (1984) [2] 260–265

[12] Xiao, L. et al.: Synthesis and thermal stability of Cr_2AlC. J. Europ. Ceram. Soc. 31 (2011) [8] 1497–1502

[13] Zhang, H.B.; Bao, Y.W.; Zhou, Y.C.: Current status in layered ternary carbide Ti_3SiC_2, a review. J. of Mater. Sci. Technol. **25** (2009) [1] 1–38

[14] Wuchina, E. et al.: UHTCs: Ultra-high temperature ceramic materials for extreme environment applications. The Electrochem. Soc. Interface **4** (2007) [4] 30–36

[15] Prescott, R.; Graham, M.J.: The formation of aluminum oxide scales on high-temperature alloys. Oxidation of Metals **38** (1992) [3/4] 233–254

[16] Hindam, H; Whittle, D.P.: Microstructure, adhesion and growth kinetics of protective scales on metals and alloys. Oxidation of Metals **18** (1982) [5/6] 245–284

[17] Grabke, H.J.: Oxidation of NiAl and FeAl. Intermetallics **7** (1999) [7] 1153–1158

[18] Zhang, H.B.; et al.: Improving the oxidation resistance of Ti_3SiC_2 by forming a $Ti_3Si_{0.9}Al_{0.1}C_2$ solid solution. Acta Materialia **52** (2004) [12] 3631–3637

[19] Lee, W.E.; Zhang, S.; Karakus, M.: Refractories: Controlled microstructure composites for extreme environments. J. of Mater. Sci. **39** (2004) [22] 6675–6685

[20] Cui, B.; Jayaseelan, D.D.; Lee, W.E.: Microstructural evolution during high-temperature oxidation of Ti_2AlC ceramics. Acta Materialia **59** (2011) [10] 4116–4125

[21] Cui, B.; Jayaseelan, D.D.; Lee, W.E.: TEM study of the early stages of Ti_2AlC oxidation at 900 °C. Scripta Materialia **67** (2012) [10] 830-833

[22] Cui, B. et al.: Microstructural evolution during high-temperature oxidation of spark plasma sintered Ti_2AlN ceramics. Acta Materialia **60** (2012) [3] 1079–1092

[23] Katsman A.; Grabke H.J.; Levin L.: Penetration of oxygen along grain boundaries during oxidation of alloys and intermetallics. Oxidation of Metals **46** (1996) [3/4] 313–331

[24] Liao, T.; Wang, J.Y.; Zhou, Y.C.: Ab initio modeling of the formation and migration of monovacancies in Ti_2AlC. Scripta Materialia **59** (2008) [8] 854–857

[25] Wang, J.Y. et al.: A first-principles investigation of the phase stability of Ti_2AlC with Al vacancies. Scripta Materialia **58** (2008) [3] 227–230

[26] Liu, C.; Huntz, A.M.; Lebrun, J.L.: Origin and development of residual stresses in the Ni-NiO system: in-situ studies at high temperature by X-ray diffraction. Mater. Sci. Engin. B **160** (1993) 113–126

[27] Kim, H.C. et al.: Crack healing, reopening and thermal expansion behavior of Al_2TiO_5 ceramics at high temperature. J. of the Europ. Ceram. Soc. **27** (2007) [2–3] 1431–1434

[28] Barsoum, M.W.: Fundamentals of Ceramics. New York 1997

[29] Byeon, J.W. et al.: Microstructure and residual stress of alumina scale formed on Ti_2AlC at high temperature in air. Oxidation of Metals **68** (2007) [1/2] 97–111

[30] Sundberg, M. et al.: Alumina forming high temperature silicides and carbides. Ceram. Int. **30** (2004) [7] 1899–1904

[31] Whittle, K. et al.: Radiation tolerance of Mn+1AXn phases, Ti_3AlC_2 and Ti_3SiC_2. Acta Materialia **58** (2010) [13] 4362–4368